Available online at www.sciencedirect.com
ScienceDirect
Energy Reports 8 (2022) 286–295
www.elsevier.com/locate/egyr

The 5th International Conference on Electrical Engineering and Green Energy, CEEGE 2022, 8–11 June, Berlin, Germany

Topologies comparison and rotor optimization of the hybrid axial transverse flux permanent magnet motor

Pengcheng Ma, Yong Li, Qian Wang*, Jianhui Hu

Electrical Engineering Department, Harbin Institute of Technology, Harbin 150001, China

Received 16 July 2022; accepted 5 August 2022
Available online xxxx

Abstract

With the advantages of high power density, the hybrid axial transverse flux permanent magnet motor (HATF-PMM) is investigated in this paper. Eight topologies of the novel HATF-PMM are proposed, analysed and compared. The applicable scopes of different topologies are summarized and the optimal topology is selected. Based on the characteristics of hybrid flux motor, an indirect optimization method through magnetic circuit decoupling and recombination is proposed. The rotor parameter optimization is performed by the proposed indirect optimization method. In the end, the HATF-PMM scheme with high power density is obtained, and the optimization law of HATF-PMM rotor parameters is revealed through the optimization process, which proves that the HATF-PMM has great potential in the application of more-electric aircraft.

Peer-review under responsibility of the scientific committee of the 5th International Conference on Electrical Engineering and Green Energy, CEEGE, 2022.

Keywords: High power density; Hybrid axial transverse flux; Indirect optimization method; Permanent magnet motor; Topologies comparison

1. Introduction

The development of transportation electrification is of great significance to the application of green energy, among which aircraft electrification requires high power density of aircraft motors [1,2]. There are many ways to improve the motor power density, among which hybrid flux motor (HFM) structure is a common way [3,4]. In [5], a dual stator radial flux permanent magnet motor and a dual stator axial flux permanent magnet motor are proposed. The same radial flux or axial flux of proposed motors with ferrite permanent magnets (PM) are coupled in the rotor, so that the power density can be significantly improved to reach the performance of the third-generation Toyota Prius with rare-earth PMs. In [6], a novel hybrid flux permanent magnet motor is proposed to increase the power density by combining the radial flux motor and axial flux motor. In [7], topologies of various hybrid flux motors are analysed, and the hybrid axial–axial flux motor is considered to have the highest power density. HFMs with axial flux and radial flux have received a lot of attention, but the research of HFM with transverse flux is rarely reported.

* Corresponding author.
E-mail address: q.wang@hit.edu.cn (Q. Wang).

https://doi.org/10.1016/j.egyr.2022.08.033

Peer-review under responsibility of the scientific committee of the 5th International Conference on Electrical Engineering and Green Energy, CEEGE, 2022.

In the conventional motors with single magnetic circuit, the axial flux permanent magnet motor (AFPMM) and the transverse flux permanent magnet motor (TFPMM) both have the characteristic of high power density [8–10]. In addition, the outer rotor structure of the motor is beneficial to improve the torque density and air-cooled conditions [11]. Therefore, a hybrid axial transverse flux permanent magnet motor (HATF-PMM) with outer rotor structure combined with the above advantages arises. For HATF-PMMs, the hybrid forms of axial flux (AF) and transverse flux (TF) in the motor is different depending on the different topologies. It is necessary to analyse different topologies and select the optimal topology for the application of the HATF-PMM. In addition, based on the high power density requirements of aircraft motors, parameter optimization of the HATF-PMM to obtain higher power density has also become a key problem in the design and application.

Therefore, based on the finite element model (FEM), eight HATF-PMM topologies are compared and analysed in this paper. The applicable scope of different topological structures is summarized and the optimal topological structure is selected. Then, the HATF-PMM parameters optimization is carried out by discretization scanning optimization, and the flux distribution law of HFM is revealed during the optimization process. Finally, the HATF-PMM optimization scheme is obtained, and the finite element simulation verified performances of the optimized HATF-PMM scheme.

2. HATF-PMM topologies analysis

2.1. Topology type

A typical topology of the HATF-PMM is illustrated in Fig. 1. The motor stator is composed of C-shaped stator core and concentrated winding, and the motor rotor is composed of axial magnetic circuit rotor and transverse magnetic circuit rotor. The moving airflow generated during the aircraft movement and the rotating motion of the outer rotor provide good cooling conditions for the HATF-PMM.

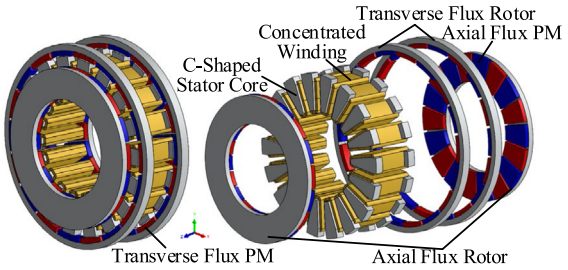

Fig. 1. The HATF-PMM typical topology.

The AF circuit and the TF circuit are mixed in the C-shaped core. The AF and the part of the winding in the slot are coupled to produce electromagnetic torque, which is similar to the principle of AFPMM. The TF and the upper end of the winding are coupled to produce electromagnetic torque. When the increase in motor power is greater than the weight increase caused by the TF circuit, the motor power density will be improved. The difference between the different topologies of the HATF-PMM lies in the structural form of the transverse magnetic circuit. Hence, the HATF-PMM can be classified into eight topologies according to the form of transverse magnetic circuit. It should be noted that the TF of different topologies enters the stator core in different forms, but the principle of coupling with winding to generate torque is the same.

First, the HATF-PMM can be classified according to the type of the TF working air gap. The structure type of HATF-PMM can be classified into R-type (radial working air gap) or A-type (axial working air gap). Then, in the range of R-type and A-type, they are further classified. According to PM mounting mode, HATF-PMM can be classified into S-type (surface PM) or I-type (interior PM). In the range of S-type and I-type, according to the direction of PM magnetization, it can be further classified into R-type (radial direction), A-type (axial direction) and T-type (tangential direction). Therefore, HATF-PMM can be classified into eight topologies according to the above classification method, as shown in Fig. 2. The eight topologies are illustrated in Fig. 3.

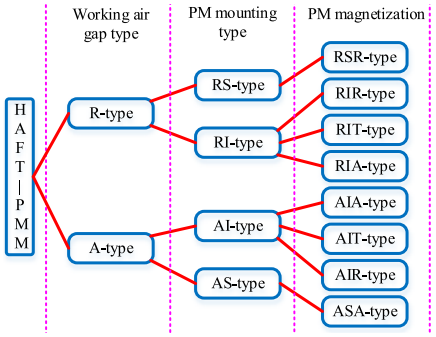

Fig. 2. The HATF-PMM topology classification.

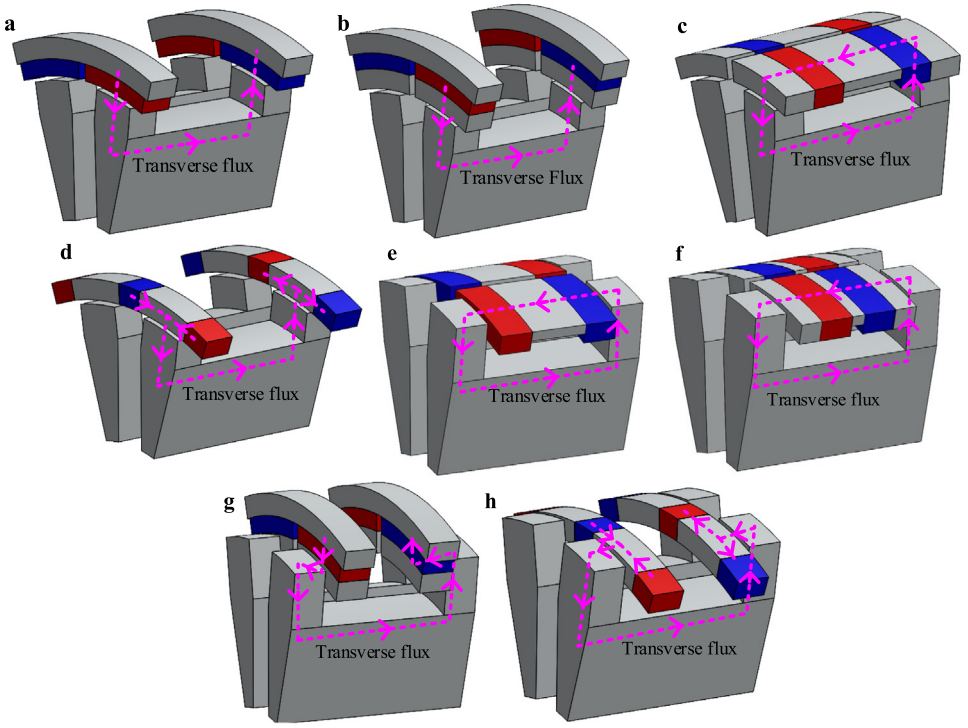

Fig. 3. Eight HATF-PMM topology types (a) RSR-type; (b) RIR-type; (c) RIA-type; (d) RIT-type; (e) ASA-type; (f) AIA-type; (g) AIR-type; (h) AIT-type.

2.2. Optimization and comparison evaluation function

Before comparing HAFT-PMM topologies, the motor performance evaluation criteria need to be defined. Different motor application fields have different performance evaluation criteria. In this paper, more-electric aircraft is taken as the application field to determine the performance concerned as power density, efficiency and motor volume. The importance of the three performance is power density greater than efficiency greater than volume. The three performances concerned by HATF-PMM are weighted by analytic hierarchy process (AHP) to construct the evaluation function of motor optimization and comparative analysis. The three performance comparison matrix and feature vectors obtained by AHP are given in Table 1, where P is the power, m is the sum of the stator and rotor weights also known as motor electromagnetic weight, η is the efficiency and V is the volume.

Table 1. Comparison matrix and feature vectors.

Parameter	*P/m*	η	*V*	Feature vectors
P/m	1	5	7	0.72351
η	1/5	1	3	0.19319
V	1/7	1/3	1	0.08331

Table 2. Comparison matrix and feature vectors.

Parameter	RSR-type	RIR-type	RIA-type	RIT-type	ASA-type	AIA-type	AIR-type	AIT-type
B_t (T)	1.03	0.67	0.60	0.72	0.98	0.59	0.46	0.64
P (kW)	6.24	5.76	5.56	5.96	6.23	5.70	5.08	5.73
η (%)	95.4	95.3	95.4	95.6	95.4	95.3	95.2	95.4
D (mm)	130.6	136	129	128	129	129	148	129
L (mm)	47.4	47.4	47.4	47.4	47.4	47.4	47.4	47.4
m (kg)	1.79	1.92	1.83	1.75	1.80	1.82	1.92	1.79
P/m (kW/kg)	3.49	2.99	3.04	3.40	3.46	3.14	2.64	3.20
F_{op} (%)	100.0	74.5	79.6	97.8	99.0	83.1	53.3	87.0

According to the feature vectors and based on the performance value of the RSR-type topology in Fig. 1, the optimization evaluation function of HATF-PMM can be defined as

$$F_{op} = \frac{0.82351 \bullet \frac{P}{m} / \frac{P_{\text{base}}}{m_{\text{base}}} - 0.19319 \bullet (1-\eta)/(1-\eta_{\text{base}}) - 0.08331 \bullet V / V_{\text{base}}}{0.72351 - 0.19319 - 0.08331} \tag{1}$$

2.3. Comparison and analysis

Based on the FEM analysis, the performance comparison of the eight topologies of the HATF-PMM with 6000 rpm speed and 6 kW power is shown in Table 2, where *D* is the maximum outside diameter of the motor, *L* is the length of the motor, and B_t is the fundamental wave amplitude of flux in transverse air gap. It should be noted that the finite element analysis of the eight topologies are performed under the same armature current condition. Therefore, the copper loss of the eight topologies is the same, but the iron loss is different with different topologies. Finally, the motor power and efficiency can be obtained by finite element analysis results.

It can be seen from Table 2 that the AIA-type, AIT-type and RIT-type topologies show good performance and have the potential of speed regulation with field weakening. However, from the absolute evaluation value of the optimization function, ASA-type and RSR-type with surface PM are considered as the optimal topologies of HATF-PMM. Based on the data of B_t, it can be seen that the surface PM topologies can generate higher fundamental wave amplitude of flux in transverse air gap under the same amount of PM. And the surface PM topology can generate more TF coupling with the armature, thus providing higher output power, which is the principle of the surface PM topologies are optimal. The ASA-type is more compact in space and has a slight advantage in motor volume, but it also brings difficulties in motor assembly. RSR-type is relatively simple in structure and easy to assemble, and has the highest evaluation value. In this paper, RSR-type is selected as the optimal topology of the HATF-PMM scheme, and further optimization research is carried out.

3. The HATF-PMM rotor pole parameters optimization

After the optimal topology of the HATF-PMM is determined, the parameters of HATF-PMM rotor poles become important parameters which have great influence on the performance. In this section, the rotor pole parameters will be optimized, and the optimal proportions of AF and TF in the main flux will be finally determined.

3.1. Influence analysis of pole pairs number

Similar to conventional permanent magnet motors, the more the pole pairs of the HATF-PMM, the smaller the yoke thickness of the rotor, the more conducive to improve the power density and reduce the motor volume.

However, the increase of the pole pairs will also increase the magnetic field frequency, resulting in a large iron loss. Compared with conventional motors, the HATF-PMM has a larger proportion of the iron loss in the loss, so it is more suitable for medium and low speed operation range. Due to the large proportion of the iron loss, the poles number of the HATF-PMM should not be too much. How to select the poles number of the HATF-PMM becomes an optimization problem that needs to balance power density, efficiency and volume at the same time.

Fig. 1 shows that the winding form of the HATF-PMM is concentrated winding, which means that the number of poles and slots of the HATF-PMM are close. For the HATF-PMM with the power of 6 kW, the appropriate number of stator slots is 18. The number of stator slots is kept as 18, and the finite element analyses are carried out for HATF-PMMs with 12 poles, 14 poles, 16 poles (the 18-pole motor windings cannot be configured), 20 poles, 22 poles and 24 poles. The parameters comparison of HATF-PMMs with different poles are shown in Fig. 4.

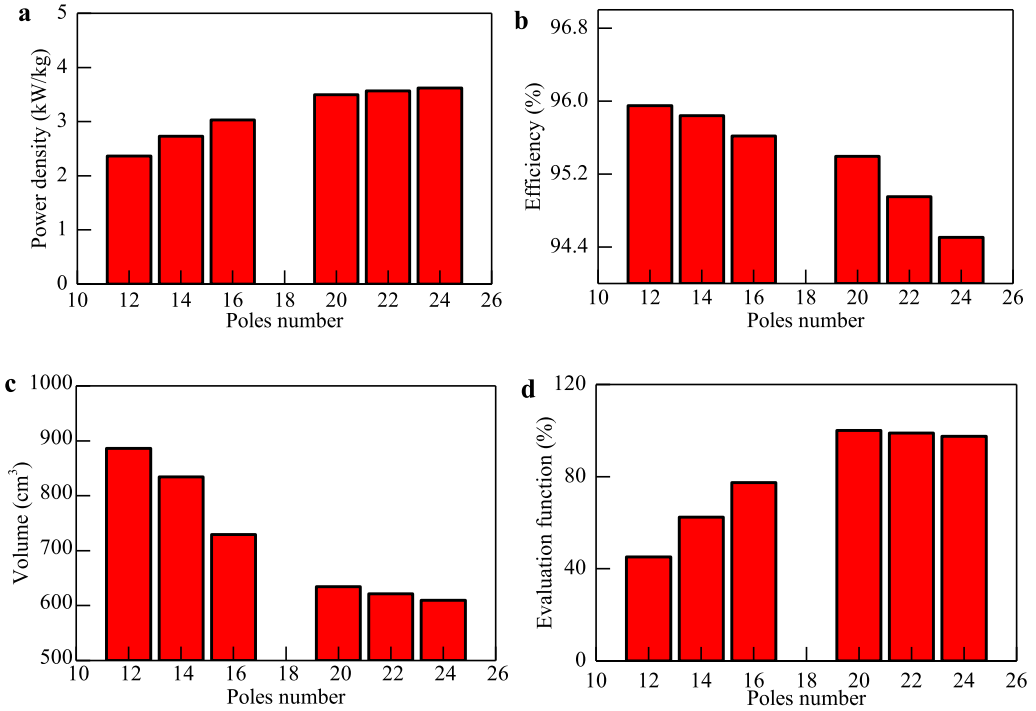

Fig. 4. Poles number influence (a) influence on power density; (b) influence on efficiency; (c) influence on volume; (d) influence on evaluation function.

As can be seen from Fig. 4, the power density of 6 kW HATF-PMM increases as the poles number increases, the efficiency decreases as the poles number increases, and the volume decreases as the poles number increases. As shown in Fig. 4(d), the optimization evaluation function results show that the optimal poles number is 20.

3.2. Optimization of arc coefficient and permanent magnet thickness

Based on the characteristic superposition of the HATF-PMM, an indirect optimization method is proposed to optimize the pole arc coefficient and permanent magnet (PM) thickness parameters. This method is different from the direct optimization method using intelligent optimization algorithm. The optimization process of the two methods is shown in Fig. 5. In Fig. 5, α_1 is the AF arc coefficient, α_2 is the TF arc coefficient, h_{m1} is the AF PM thickness, and h_{m2} is the TF PM thickness.

Considering the mechanical strength, cost and other factors of PMs, the optimization constraint of the pole arc coefficient is between 0.1 to 1, and the optimization constraint of the thickness of PM is between 2 mm to 5 mm. The variation of power and weight with parameters is shown in Figs. 6 and 7, respectively.

Combined with Figs. 6 and 7, the power density changes with parameters as shown in Fig. 8. As can be seen from Fig. 8, the decoupling power density of AF circuit and TF circuit both decrease with the increase of PM

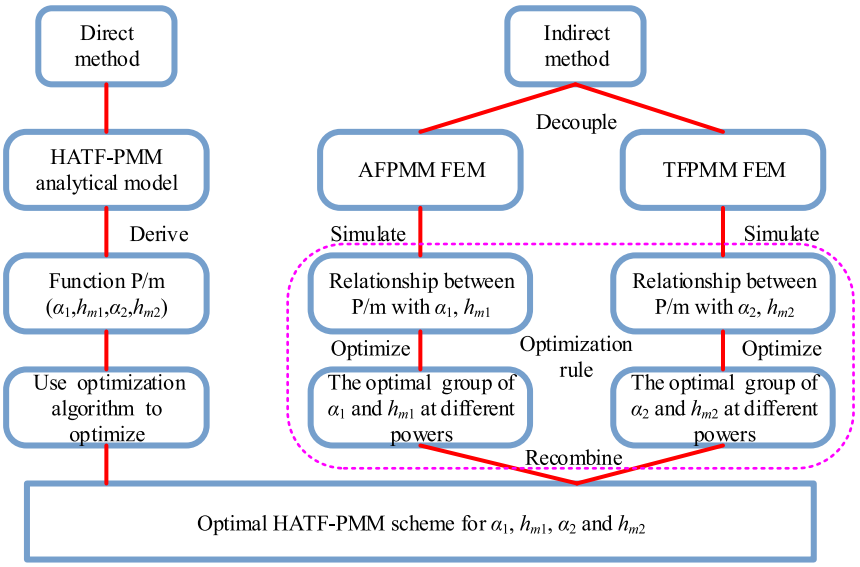

Fig. 5. The optimization process of the two methods.

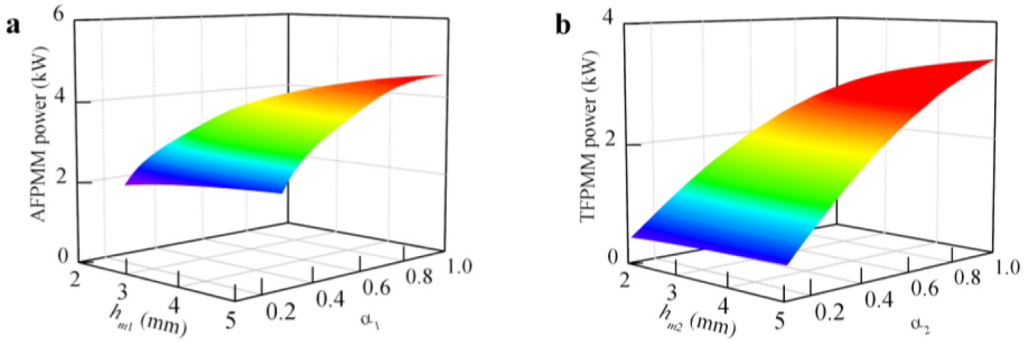

Fig. 6. (a) Influence on AF power; (b) influence on TF power.

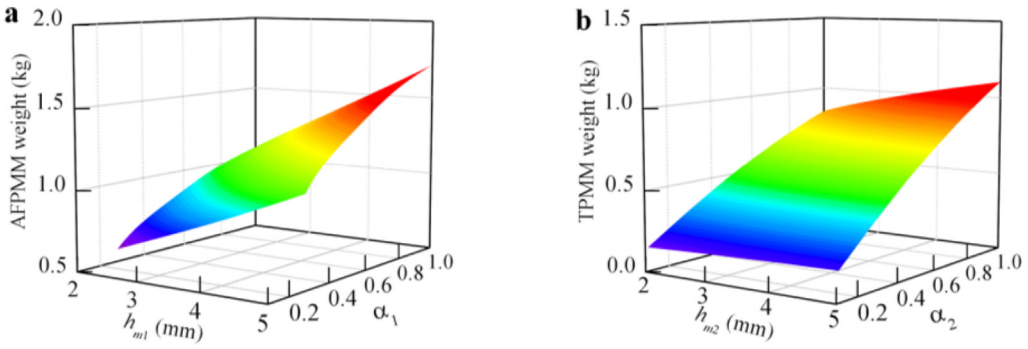

Fig. 7. (a) Influence on AF weight; (b) influence on TF weight.

thickness, and increase first and then decrease with the increase of arc coefficient. The decoupling power density of the AF circuit reaches the maximum when the arc coefficient is 0.8, and that of the TF circuit reaches the maximum

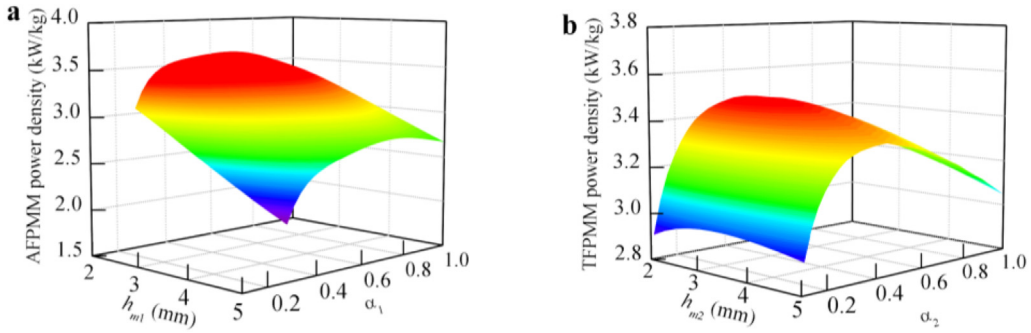

Fig. 8. (a) Influence on AF power density; (b) influence on TF power density.

when the arc coefficient is 0.45. This result is equivalent to the local optimal solution when only AF circuit or TF circuit is considered, not the global optimal solution. However, the law of the local optimal solution indicates that the arc coefficient of PMs in the AF circuit should be large, and that of PMs in the TF should be relatively small.

It should be noted that the rotor parameters are optimized in this section on the basis of the RSR-type HATF-PMM scheme in Table 2, which means that the motor stator shared by AF rotor and TF rotor does not change. After decoupling, the weight of the stator is divided between the AF and the TF according to the proportion of the flux to the main flux. When the two kinds of flux are small, the superposed flux is far less than the original main flux. At this time, the weight of the motor stator is not fully distributed to the AF and the TF, and the decoupling power density is abnormally large. This power density is called the decoupling power density and is not the true motor power density. Therefore, it is necessary to recombine the AF and TF, and take all stator weights into account to obtain the correct power density.

The same power in AF and TF may correspond to different power densities. The maximum power density is selected as the corresponding value of the power, and the parameter group of the arc coefficient and PM thickness under the power is recorded, which is called the optimal parameter group as shown in Fig. 9.

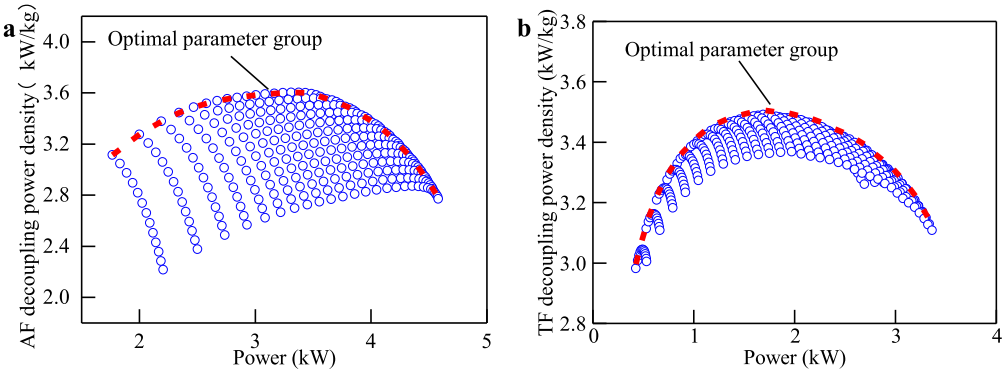

Fig. 9. (a) Relationship between power and AF power density; (b) Relationship between power and TF power density.

AFPMM and TFPMM are recombined according to the power parameters, and the power density is recalculated with all stator weight taken into account. The power groups that meets the requirements are selected, and the power group with the highest power density is found. Then, the α_1, h_{m1}, α_2 and h_{m2} of the group are obtained according to the previous records, and the power density optimization is completed. The power groups of AF circuit and TF circuit that meets the power requirements are the range represented by the narrow and long surface in Fig. 10.

In the optimal power group shown in Fig. 10, the AF power is 3.73 kW, the TF power is 2.51 kW, the total power is 6.24 kW, and the optimal power density is 3.47 kW/kg. The optimization results show that high axial flux and its power proportion is more reasonable for improving the power density in the HATF-PMM. The optimal group of arc coefficient and PM thickness are $\alpha_1 = 0.88$, $h_{m1} = 2.5$ mm, $\alpha_2 = 0.52$ and $h_{m2} = 4.5$ mm.

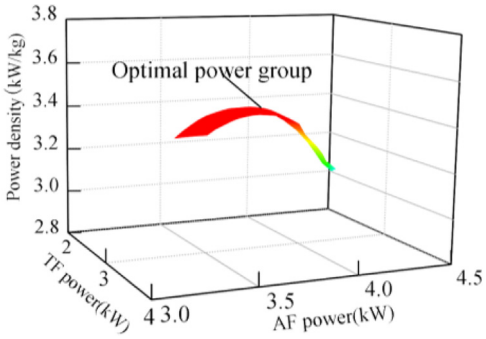

Fig. 10. The power groups that meets the requirements.

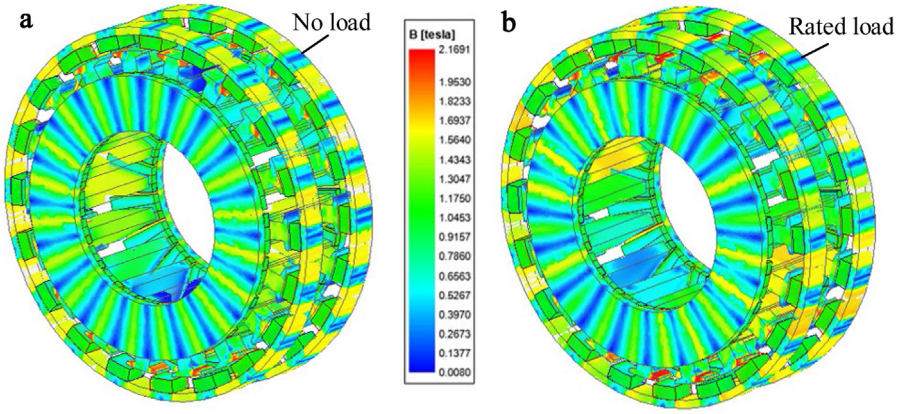

Fig. 11. (a) Magnetic field distribution of no load HATF-PMM; (b) Magnetic field distribution of rated load HATF-PMM.

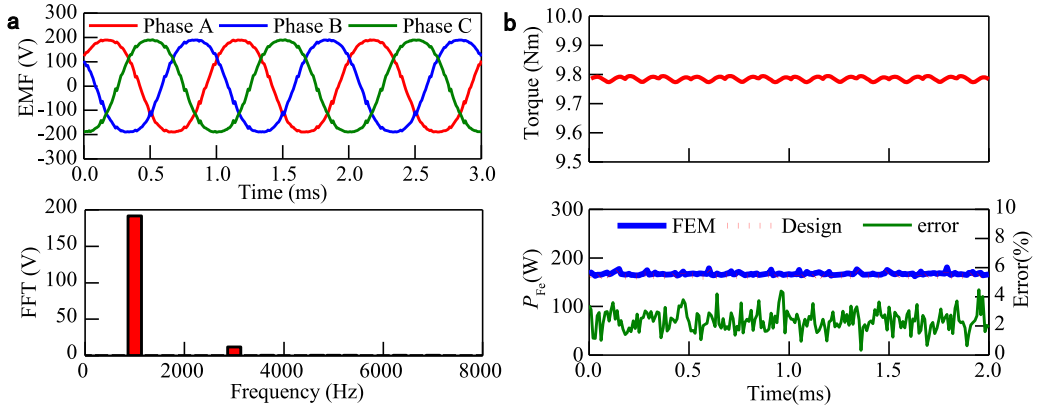

Fig. 12. (a) No-load EMF waveform and Fourier analysis; (b) Output torque and iron loss at rated load.

3.3. Optimization results

According to the optimization parameters, the recombined FEM of the HATF-PMM is established. The rated load armature current is 20 A and the FEM magnetic field distribution are shown in Fig. 11. The no load Electromotive Force (EMF), rated load torque and iron loss of the HATF-PMM are shown in Fig. 12.

Fig. 12(a) shows that the no-load EMF of the HATF-PMM has good sinusoidal property and low harmonic content. According to the torque value in Fig. 12(b), the power of the HATF-PMM at 6000 rpm is 6.14 kW,

slightly lower than the optimized design value of 6.24 kW, which is caused by the slight saturation of the stator core after AF and TF recombination. In addition, the average iron loss of the HATF-PMM is 171 W, which is about 3% higher than the design value due to saturation. It is considered that the FEM results are consistent with the optimized design values, which verifies the feasibility of the optimized method.

4. Conclusions

In this paper, eight kinds of HATF-PMM topologies have been proposed, compared and analysed, among which RSR-type with highest power density been considered to be the optimal topology for aircraft motors due to its highest fundamental wave amplitude of flux in transverse air gap. The power density of ASA-type is close to the RSR-type, but its structure is more complex. The AIA-type, AIT-type and RIT-type have application value in speed regulation with field weakening, while other types have low application value. Based on the optimal topology, the relationship between the poles number and the HATF-PMM performance has been analysed. For the HATF-PMM with 6000 rpm speed and 6 kW power, the power density of 20 poles is 47.9%, 28.1% and 15.4% higher than that of 12, 14 and 16 poles, and the efficiency is 0.4% and 0.9% higher than that of 22 and 24 poles. According to the comparison of the defined evaluation function, 20 is the optimal number of poles. In addition, an indirect optimization method through magnetic circuit decoupling and recombination is proposed, and the optimization of the arc coefficient and PM thickness has been carried out. In the indirect optimization process, it is found that the optimal AF arc coefficient is 0.88, the optimal TF arc coefficient is 0.52, the optimal AF power accounts for 60%, and the optimal TF power accounts for 40%. Finally, the HATF-PMM optimization scheme is obtained, and performances of the optimized HATF-PMM scheme are verified by finite element simulation. Due to saturation of the stator core after the AF and TF recombination, the power of the HATF-PMM is 1.6% lower and iron loss is 3% higher than the design value, which is considered within the permissible margin of error. The results prove that the proposed optimization method has high accuracy and application value, and the optimization design results can be used for reference in the design, optimization and application of the HATF-PMM.

CRediT authorship contribution statement

Pengcheng Ma: Investigation, Formal analysis, Validation, Writing – original draft. **Yong Li:** Writing – review & editing. **Qian Wang:** Data curation, Writing – review & editing. **Jianhui Hu:** Conceptualization, Supervision, Writing – review & editing, Project administration, Funding acquisition.

Declaration of competing interest

The authors declare that they have no known competing financial interests or personal relationships that could have appeared to influence the work reported in this paper.

Data availability

Data will be made available on request.

Acknowledgment

This work was supported by Self-Planned Task(NO. SKLRS202008B) of State Key Laboratory of Robotics and System (HIT).

References

[1] Benzaquen J, He J, Mirafzal B. Toward more electric powertrains in aircraft: Technical challenges and advancements. CES Trans Electr Motors Syst 2021;5(3):177–93.

[2] Zhao E, Song S, Ma Z, Zhang X, Ning L, Liu Y. Design and initial testing of an integrated switched reluctance starter/generator system for unmanned aerial vehicle. CES Trans Electr Mach Syst 2018;2(4):377–83.

[3] Zhao H, Liu C, Song Z, Liu S. Design and control of a new compound double-rotor electric motor for hybrid propulsion system. IEEE Trans Power Electron 2022;37(3):3283–96.

[4] Chen X, Wang J, Griffo A, Spagnolo A. Thermal modeling of hollow conductors for direct cooling of electrical machines. IEEE Trans Ind Electron 2020;67(2):895–905.

[5] Zhao W, Lipo TA, Kwon B. Comparative study on novel dual stator radial flux and axial flux permanent magnet motors with ferrite magnets for traction application. IEEE Trans Magn 2014;50(11):1–4.
[6] Seo JM, Ro J, Rhyu S, Jung I, Jung H. Novel hybrid radial and axial flux permanent-magnet motor using integrated windings for high-power density. IEEE Trans Magn 2015;51(3):1–4.
[7] Liu Y, Cheng D, Bai J, Tong C, Song Z, Tong W. Topology comparison of compound-structure permanent-magnet synchronous motors. IEEE Trans Ind Appl 2012;48(6):2217–22.
[8] Kurt Erol, Gör Halil, Demirtaş Mehmet. Theoretical and experimental analyses of a single phase permanent magnet generator (PMG) with multiple cores having axial and radial directed fluxes. Energy Convers Manage 2014;77:163–72.
[9] Zhang W, Lin M, Xu D, Fu X, Hao L. Novel fault-tolerant design of axial field flux-switching permanent magnet machine. IEEE Trans Appl Supercond 2014;24(3):1–4.
[10] Zhang W, Xu Y, Zhou G. Research on a novel transverse flux permanent magnet motor with hybrid stator core and disk-type rotor for industrial robot applications. IEEE Trans Ind Electron 2021;68(11):11223–33.
[11] Mbadiwe Enwelum I, Sulaiman Erwan Bin. Design and optimization of outer-rotor permanent magnet flux switching motor using transverse segmental rotor shape for automotive applications. Ain Shams Eng J 2021;12(1):507–16.